Met. Mater. Int., Vol. 17, No. 1 (2011), pp. 99~104
doi: 10.1007/s12540-011-0213-1 Published 26 February 2011

Variations in Electrical and Physical Properties of Al:ZnO Films with Preparation Conditions

J.-I. Son[1], J.-H. Shim[2], and N.-H. Cho[1,*]

[1]Department of Materials Science and Engineering, Inha University, Incheon 402-751, Korea
[2]Department of Materials Science and Engineering, University of Washington, Seattle, WA 98195, USA

(received date: 19 January 2010 / accepted date: 5 October 2010)

This study examined the effects of the RF magnetron sputtering power and substrate temperature on the electrical and physical properties of Al:ZnO (AZO) thin films deposited on GaAs(011) and Si(001) substrates. The stress on the films, which was estimated by determining the position of the (002) XRD diffraction peaks, varied from 5.28 GPa to 2.29 GPa for the films deposited between 100 and 250 W RF power. A similar trend was observed for the films prepared at substrate temperatures ranging from R.T. to 300 °C. The films prepared at 100 °C showed the least amount of stress and the largest concentration of charge carriers. The concentration of charge carriers produced from the presence of $[Al_{Zn}]$ is closely related to the stress on the films. Post-deposition annealing in a reducing atmosphere had not only decreased the compressive stress, but had also formed oxygen vacancies. The increased concentration of charge carriers after annealing was attributed to the ionization of oxygen vacancies with a probability of 0.1±0.03.

Keywords: thin films, annealing, sputtering, electrical properties, residual stress

1. INTRODUCTION

Transparent conducting oxides (TCO) with a wide-band gap, such as indium tin oxide (ITO) and zinc oxide (ZnO), have attracted considerable interest in electro-optic industries because of their unique and useful optical and electrical properties. These oxides can be used as electrodes in display panels, solar cells, gas sensors, and a range of other light emitting devices [1-4]. There has been an increase in interest in replacing expensive ITO with ZnO in displays and electric transducers due to its low toxicity and excellent TCO properties, such as an electrical resistivity and optical transmittance of $1 \times 10^{-3}\Omega$/cm and > 90 %, respectively.

The n-type electrical conductivity of semiconducting ZnO is associated with nonstoichiometry, including zinc interstitials, oxygen vacancies, and a substitutional solid solution. Therefore, there have been two different approaches to enhance the electrical conductivity: replacing Zn^{2+} ions with elements, such as Al^{3+}, Ga^{3+} and In^{3+}, etc. [5-7], or post-deposition annealing in a reducing atmosphere to control the concentration of oxygen vacancies [8].

Most thin films tend to be under stress because of the lattice parameter and thermal expansion coefficients differentiating between the films and the substrate. The stress on the films affects the structural and electrical properties. In particular, the solubility limit of Al^{3+}, Ga^{3+} and In^{3+} substituents in ZnO is affected by the stress on the films. However, it is unclear how the stress affects the electrical properties and doping efficiency. The distortion of the unit cell under compressive stress would vary the solubility limit. For example, doping ions that are larger than Zn at the Zn atomic sites, such as Ga or In, would be preferred under tensile stress. Therefore, it is essential to understand how the stress varies with the deposition conditions and doping features of the film.

In this study, AZO films were prepared by RF magnetron sputtering on GaAs and Si substrates. The stress on the films was estimated in terms of the preparation conditions, such as the sputtering power, substrate temperature, and post-deposition annealing. This study examined the effects of post-deposition annealing under a reducing oxygen atmosphere on the electrical and structural properties. The change in carrier concentration was examined and found to be related to the stress-dependent solubility limit of the dopants.

2. EXPERIMENTAL PROCEDURE

An Al-doped ZnO target was used as the source for the AZO thin film deposition. The target was synthesized by sintering a mixture of 98 wt.% ZnO and 2 wt.% Al_2O_3 at 1400 °C for 4 h, while suspended in the air. Thin films were

*Corresponding author: nhcho@inha.ac.kr
©KIM and Springer

Table 1. Deposition Condition of the AZO Thin Films

Deposition parameter	Experimental range
target(2"×1/6")	Al:ZnO(AZO)
substrate	Si wafer, GaAs wafer
sputter power(watt)	100~250 (RF)
Background pressure (Torr)	1×10^{-5}
working pressure (Torr)	5×10^{-2}
substrate temperature (°C)	R.T.~300

deposited on GaAs and Si substrates by RF magnetron sputtering. Three different types of films were prepared: (i) films deposited by sputtering in the range of 100 W to 250 W RF at R.T. (group A); (ii) films prepared at substrate temperatures between R.T. and 300 at 150 W RF (group B); and (iii) films prepared at 150 W RF and 100 °C, and then annealed at various oxygen pressures ($1.5\times10^{2}\sim1.0\times10^{-6}$ Torr) at 400 °C for 1 h (group C). Table 1 shows the deposition conditions used to produce the three different groups of AZO thin films.

The structural properties were examined by synchrotron X-ray scattering measurements at the 8C1 POSCO beamline at Pohang Light Source (PLS) in Korea. Chemical analysis was carried out by X-ray photoelectron spectroscopy (XPS, Thermo Scientific K-Alpha). Microstructural and morphological features of the films were analyzed by FE-SEM (Hitachi S-4300SE). The electrical properties, such as the concentration and mobility of the charge carriers, and the electrical conductivity were measured using a 4-point probe-station and Hall-measurement system.

3. RESULTS

3.1. Influence of sputtering power

Figure 1 shows the XRD patterns of the group A films. The characteristic features of the XRD patterns varied depending on the sputtering power. The intensity of the (002) diffraction peak increased significantly as the sputtering power increased from 100 W to 150 W, and the (101), (102), (100), and (110) peaks were observed clearly. However, when the sputtering power was > 200 W, the (002) peak began to narrow as the sputtering power increased, while the intensity of the other peaks decreased significantly and some disappeared altogether. This suggests that the preferential orientation parallel to the (002) and (101) is affected by the sputtering power. The inset illustrates the deposition rate, as well as the full-width at half-maximum (FWHM) of the (002) peaks of the films. The crystallinity and deposition rates of the films increased with the increasing sputter power. The grain size of the films was estimated using the Scherrer equation:

$$D(\text{crystallite size}) = \frac{0.9\lambda}{B\cdot\cos\theta} \quad (1)$$

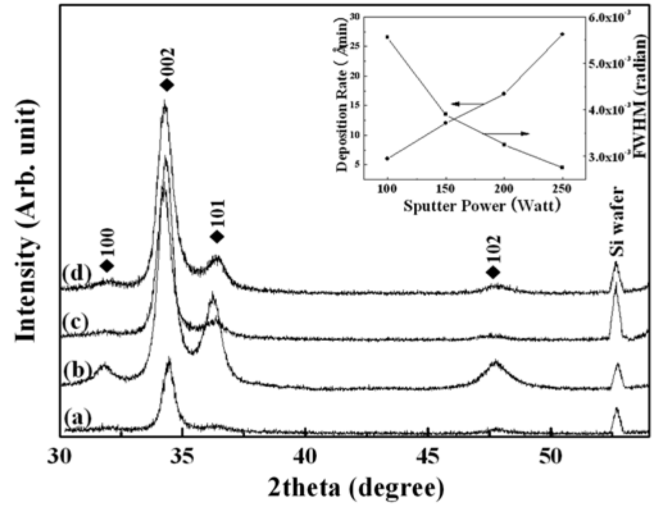

Fig. 1. XRD patterns of the films in group A. The films were prepared at RF powers ranging from 100 W to 250 W; the substrate temperature was R.T. Spectra (a), (b), (c) and (d) were obtained from the films prepared at sputtering powers of 100 W, 150 W, 200 W, and 250 W, respectively. The inset illustrates the change in deposition rate of the films and the FWHM of the (002) peaks in the XRD patterns as a function of the sputtering power.

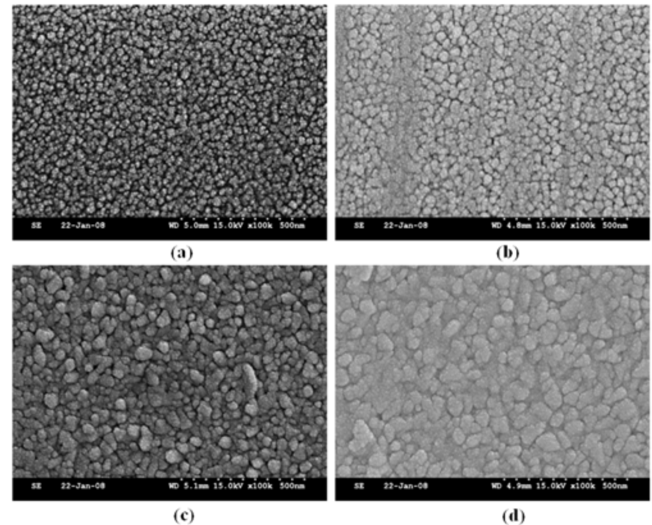

Fig. 2. SEM images of the films in group A. The films were prepared at sputtering powers of 100 W (a), 150 W (b), 200 W (c), and 250 W (d), respectively.

In this equation, λ is the X-ray wavelength and B is the FWHM. The calculated crystallite sizes were confirmed by the SEM images' plane-view estimate of the crystallite sizes, as seen in Fig. 2. The grain size increased from 28 nm to 56 nm, with an increase in sputtering power from 100 W to 250 W. Figure 3 shows the electrical properties as a function of the sputtering power. The electrical resistivity and hall mobility of the films tends to increase as the sputtering power increases, whereas the carrier concentration was relatively constant at $\sim2.5\times10^{20}/cm^3$ between 100 W to 200 W,

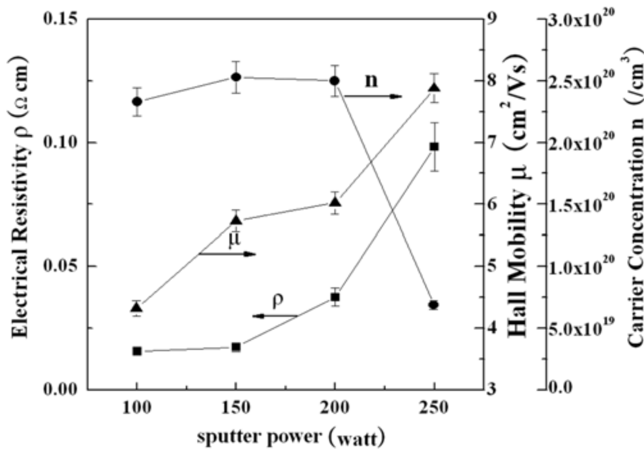

Fig. 3. Variation in the electrical properties of the AZO thin films with the sputtering power. The films were prepared at sputtering powers ranging from 100 W to 250 W; the substrate temperature was R.T.

but decreased to ~5 × 10^{19}/cm^3 at 250 W. The films were deposited at 150 W, and those samples showed the highest electrical conductivity.

3.2. Effect of the substrate temperature

Figure 4 shows the XRD patterns of the films from group B. The films mostly grew perpendicularly from the substrate surface, with a columnar-shape in the c-axis. Additionally, the (101), (102), and (100) peaks were observed. The FWHM of the (002) XRD peaks of the films appeared to vary with the substrate temperature, as shown in the inset. The FWHM changed from 3.9 × 10^{-3} to 3.4 × 10^{-3} radian

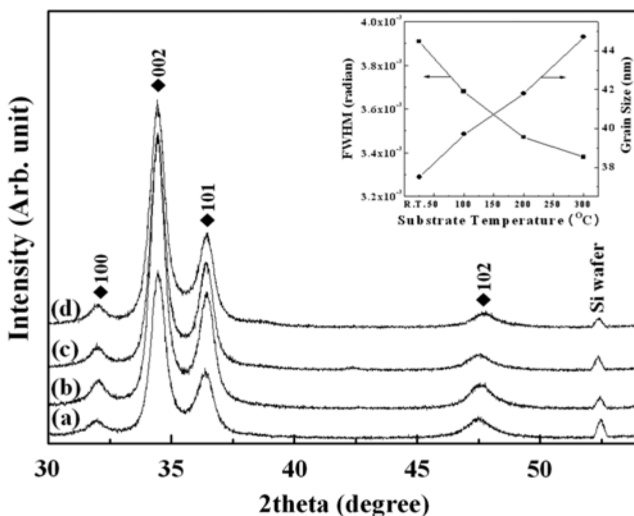

Fig. 4. XRD patterns of the films in group B. The films were prepared at substrate temperatures ranging from R.T. to 300 °C. The sputter power was 150 W. Spectra (a), (b), (c), and (d) were obtained from the films prepared at substrate temperatures of R.T., 100 °C, 200 °C, and 300 °C, respectively. The inset illustrates the change in the FWHM of the (002) peaks and the grain size as a function of the substrate temperature.

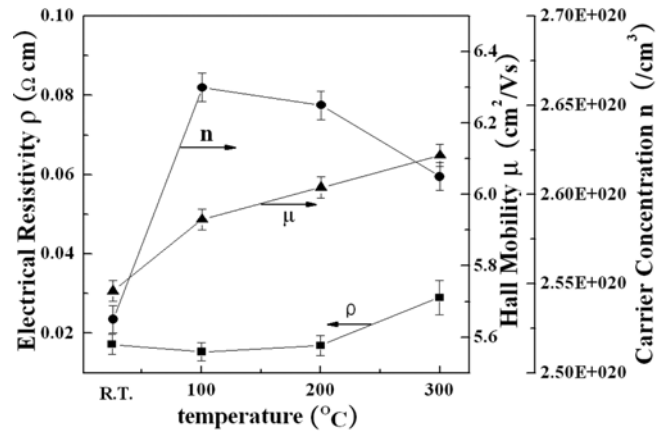

Fig. 5. Variation in the electrical properties of the AZO thin films with the substrate temperature. The films were prepared at 150 W.

and the grain size increased from 37.5 nm to 43.5 nm as the substrate temperature increased from R.T. to 300 °C. Figure 5 shows the electrical properties of the group B films as a function of the substrate temperature. The mobility of the charge carriers increased from 5.7 cm^2/Vs to 6.1 cm^2/Vs as the substrate temperature increased. This appears to match the microstructural changes in the films due to the substrate temperature. The enhanced crystallinity and grain growth contributed to the higher mobility of the charge carriers.

On the other hand, the concentration of electrons increased to a maximum value when the substrate temperature increased from R.T. to 100 °C, and then decreased upon an increase in temperature. The resistivity decreased as the temperature increased from R.T. to 100 °C; the resistivity was 0.03 Ω/cm at 300 °C.

3.3. Variations on the stress of the film with preparation conditions

Figure 6 shows the variations in the (002) peak positions of the XRD patterns obtained from the film groups A, B, and C. In Fig. 6(a), spectra ①, ②, ③, and ④ were recorded from the films prepared at sputtering powers of 100 W, 150 W, 200 W, and 250 W, respectively.

In Fig. 6(a), the maximum position (2θ) varied from 34.00° to 34.23°. All of these peaks indicate the presence of stress on the films when compared to the (002) peak at 34.40° (c = 5.210Å) for a strain–free ZnO crystal. Of all the films, those prepared at 150 W appeared to have a (002) peak at the highest angle compared to the other films prepared at 100 W, 200 W, and 250 W.

In Fig. 6(b), spectra ①, ②, ③, and ④ were recorded from the films prepared at R.T., 100, 200 °C, and 300 °C, respectively. These spectra illustrate the change in the maximum position of the (002) XRD peak as the substrate temperature varied from R.T. to 300 °C at 150 W; the maximum position shifted from 34.23° to 34.27°. The highest angle of

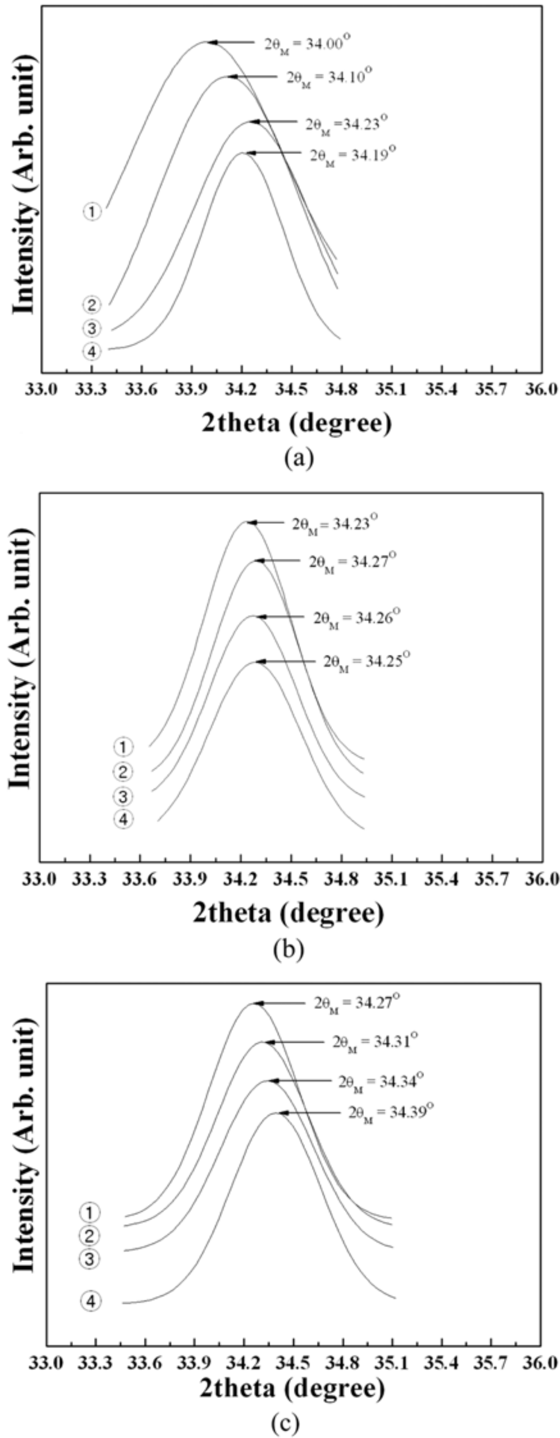

Fig. 6. Variation in the (002) peak position in the XRD patterns; these patterns were obtained from the films of groups A (a), B (b), and C (c), respectively. (a) Spectra ①, ②, ③, and ④ were recorded from the films prepared at sputtering powers of 100, 150, 200, and 250 W, respectively. (b) Spectra ①, ②, ③, and ④ were obtained from the films prepared at R.T., 100, 200, and 300, respectively. (c) Spectra ①, ②, ③, and ④ were recorded from the films which were prepared at a sputtering power of 150 w at 100 °C and then post-deposition annealed under oxygen pressures of 1.5×10^2, 2.0×10^{-2}, 5.0×10^{-3}, and 1.0×10^{-6} Torr, respectively.

34.27° was obtained for the films prepared at a substrate temperature of 100 °C.

In Fig. 6(c), spectra ①, ②, ③, and ④ were obtained from the films that were prepared at a sputtering power of 150 W at 100 °C, and then post-deposition annealed under oxygen pressures of 1.5×10^2 Torr, 2.0×10^{-2} Torr, 5.0×10^{-3} Torr, and 1.0×10^{-6} Torr, respectively.

These peaks illustrate that the (002) peak position shifted from 34.28° to 34.39°, due to a decrease in oxygen pressure. The variation in the lattice parameter indicated that each film was prepared under a particular stress depending on the different annealing conditions.

The stress on the AZO films was calculated based on the position of the (002) peaks from the following formula [9-11]:

$$\sigma(stress) = -453.6 \times 10^9((c - c_0)/c_0) \quad (2)$$

In this formula, c_0 is 5.210Å (c-axis lattice parameter, for standard ZnO) and c is the measured c-axis parameter from the post-deposition annealed thin films.

Table 2 shows the change in the (002) peak angles with the sputtering power, substrate temperature, annealing conditions, and calculated stress on the films. The AZO films grown at 150 W appeared to have the largest lattice parameter (5.2304Å), which decreased to that of the strain-free lattice parameter (c_0 = 5.2093Å) when the films were annealed at 1.0×10^{-6} Torr.

Figure 7 shows the change in the fraction [O/Zn] and the concentration of charge carriers. The ratio of O to Zn atoms was estimated by an X-ray photoelectron spectroscopy. The peaks corresponding to Zn 3p and O 1s electron orbital were chosen and their intensities were used for measurements [12]. The variation in the non-stoichiometric factor with the Po_2 partial pressure was approximately 0.016. The concentration of charge carriers increased by approximately 0.7×10^2 /cm^3 after annealing at 1.0×10^{-6} Po_2 Torr; annealing at low oxygen pressures showed a decrease of electrical resistivity. The mobility of the charge carriers increased as annealing decreased the Po_2 pressure, however the change was small ($\Delta\mu$ = 0.4 cm^2/v·s) [11,13].

4. DISCUSSION

4.1. Change in the electronic properties due to film deposition conditions

The change in the mobility appears to match the change in the microstructural features of the films. The mobility was enhanced as the grain became larger and the crystallinity improved. The value was doubled when the power was increased from 100 W to 250 W. In contrast, the carrier concentration was relatively constant over the sputtering power range, 100 W to 250 W, and decreased from 2.5×10^{20}/cm^3

Table 2. Mechanical Stress of the AZO Films with Sputtering Power, Substrate Temperature, and Post-Deposition Annealing Atmosphere

	Sputter power (W)				Substrate temperature (°C)				Po_2 (Torr)			
	100	150	200	250	R.T.	100	200	300	1.5×10^{2}	2.0×10^{-2}	5.0×10^{-3}	1.0×10^{-6}
peal angle (degree)	34.19	34.23	34.10	34.00	34.23	34.27	34.26	34.25	34.28	34.31	34.34	34.39
c-axis lattice parameter (Å)	5.2434	5.2363	5.2557	5.2706	5.2363	5.2304	5.2319	5.2333	5.2284	5.2211	5.2167	5.2093
Compressive stress (GPa)	2.79	2.20	3.98	5.28	2.29	1.77	1.90	2.03	1.61	1.23	0.85	0.20
Carrier concentration ($\times10^{20}/cm^3$)	2.36	2.53	2.50	0.71	2.53	2.66	2.64	2.61	2.83	3.02	3.11	3.52

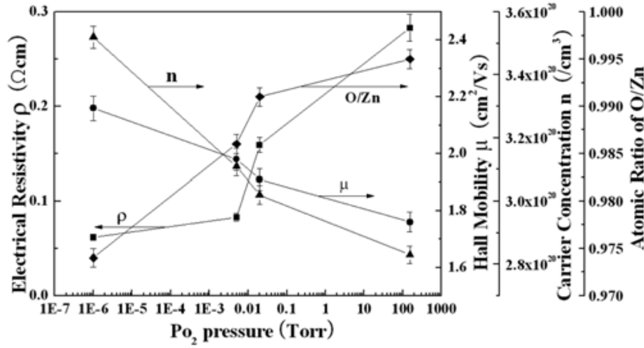

Fig. 7. Variation in the electrical properties and oxygen vacancy fraction as a function of the oxygen partial pressure under which the film was post-deposition annealed.

to $7 \times 10^{19}/cm^3$ when the grain size increased from 28 nm to 56 nm.

The majority of the carriers, which are electrons in the conduction band, originated from the substitution of Zn with Al; this substitution appears to have been affected by the sputtering power. There was little variation in substitution when the sputtering power was between 100 W to 200 W, however, there was a significant decrease in substitution at 250 W. The films prepared at 150 W showed the highest concentration of electrons. It is highly likely that the variation in the carrier concentration is related to the change in the solubility of Al at the Zn atomic sites. Al is less likely to remain at the atomic sites of Zn as sputtering power increases to 250 W. Instead, it can be migrated to regions like the grain boundaries, interface, and surface. Segregation phenomena, such as this, have been observed in solid solutions when the solubility is limited. Therefore, the carrier concentration in the films under high stress decreased when the films were deposited at 250 W.

The electrical conductivity appears to be affected mainly by the carrier concentration. This is why the electrical conductivity decreased when the sputtering power increased from 200 W to 250 W, even though the mobility was enhanced. Also, increasing the sputter power raises the film's growth rate. It is likely that within the sputtering power range, the kinetic energy of the sputtered particles arriving at the substrate surface increases monotonously as the power increases. This provides the adsorbed particles with a higher surface mobility. Additionally, this leads to an increase in grain size and enhanced crystallinity.

As the substrate temperature increased from R.T. to 300 °C, the grain size increased to 45 nm, and the crystallinity increased with the surface mobility of sputtered particles. In contrast, the concentration of charge carriers, which are generated from the substitution of Zn with Al, reached its maximum value in the film prepared at 100 °C, but then decreased with an increasing substrate temperature. This was closely related to the formation of a solid solution. The solubility limit appears to decrease as temperatures increase from 100 °C to 300 °C, and the maximum concentration of carriers was observed in the films prepared at a substrate temperature of 100 °C. Therefore, the highest electrical conductivity was achieved, even though the carrier mobility was lower than that of the films prepared at 200 °C and 300 °C.

4.2. Effects of stress on the physical properties of the films

All the films prepared in this experiment contained a particular amount of Al as a substitutional element. This substitution is believed to produce charge carriers related to the production of defects, such as $[Al_{Zn}]$. The atomic fraction of Al in the films was approximately 0.016, based on the chemical analysis of the films. However, the observed carrier concentration of $2.4 \times 10^{20}/cm^3$ to $2.5 \times 10^{20}/cm^3$ was lower than the expected results of the films prepared at R.T., with a sputtering power of 100 W to 200 W. In particular, the film deposited at 250 W had a carrier concentration of $7 \times 10^{19}/cm^3$.

The XRD of this film revealed the (002) peak at ~34.00°. The film is under a compressive stress of 0.20 GPa, considering the value of 34.39°, where c = 5.2093Å; this appears to affect the substitution of Zn with Al. The radius of Al^{3+} is 0.2Å smaller than that of Zn^{2+}. The level of substitution decreased significantly as the compressive stress varied from 3.98 GPa (34.10° 2θ) to 5.28 GPa (34.00° 2θ). This was observed when the sputter power was increased from 200 to 250 W.

The film prepared at 150 W appeared to have the least amount of stress among the films of group A, as shown Fig. 1. It is likely that the substitution of Zn with Al occurred most efficiently when the films were prepared at 150 W, producing the highest concentration of conducting electrons in group A.

The (002) peaks of the films prepared at substrate temperatures from R.T. to 300 °C were observed at 34.23° to 34.27°, and the carrier concentration ranged from $2.70 \times 10^{20}/cm^3$ to $2.83 \times 10^{20}/cm^3$. There appears to be a slight variation in the

degree of substitution of Zn with Al under this compressive stress range. The largest carrier concentration appeared on the film prepared at 100 °C. The corresponding (002) peak was observed at 34.27°, which is larger than that of the other films in group B. The film conductivity is affected by the carrier mobility, which appears to be determined by the microstructure.

The O/Zn ratio in Fig. 7 suggests that the oxygen vacancy fraction, $[V_O]$, varied from 5×10^{-3} to 25×10^{-3} with a decreasing oxygen pressure (Po_2) from 1.5×10^2 Torr to 1.0×10^{-6} Torr. The formation of oxygen vacancies is another source of mobile electrons. Some of the carriers are believed to be produced by the ionization of oxygen vacancies.

If an oxygen vacancy is ionized to produce charge carrier electrons, the concentration will increase when the film is heat-treated at an oxygen pressure (Po_2) of 1.5×10^2 Torr to 1.0×10^{-6} Torr. The value corresponding to the charge carriers, $0.17 \times 10^{20}/cm^3$ to $0.86 \times 10^{20}/cm^3$, is related to the concentration of oxygen vacancies, $2.1 \times 10^{20}/cm^3$ to $10.5 \times 10^{20}/cm^3$ by a multiple of 0.1 ± 0.03. This suggests that the oxygen vacancies are ionized with a probability factor of 0.1 ± 0.03, which indicates a shift in the Fermi level [14-18].

For the films that are post-deposition annealed under a reducing atmosphere, the (002) peak varied from 34.28° to 34.39°. The c-axis parameter was similar to that of a single crystallite ZnO with little stress. The compressive stress appeared to disappear as oxygen vacancy concentration increased due to the heat-treatment under a reducing atmosphere. Very little stress was observed in the films heat-treated at an oxygen pressure of 1×10^{-6} Torr. The presence of such compressive stress does not appear to have any noticeable effect on the substitution of Zn with Al at varying atmospheres.

The change in the carrier concentration of the films prepared at 150 W, 100 °C, and post-deposition annealed can be explained by the change in the concentration of oxygen vacancies. Additionally, it had an ionization probability factor of 0.1 ± 0.03, with a carrier concentration of $2.66 \times 10^{20}/cm^3$ due to the substitution of Zn with Al .

5. CONCLUSION

Al-doped ZnO thin films were prepared by RF magnetron sputtering. The effects of the sputtering power and substrate temperature on the electrical properties and the generation of carriers were examined. The stress on the films was estimated by determining the position of the (002) XRD peak. The stress varied from 5.28 GPa to 2.29 GPa for the films prepared at the sputtering powers ranges of 100 W to 250 W. The largest carrier concentration and highest conductivity were observed in the films showing the least amount of stress. The solubility limit, at which Al can substitute for Zn, appears to be closely related to the stress on the film; less stress equals a higher solubility.

A similar trend was observed for the films prepared at the substrate temperatures ranging from R.T. to 300 °C. The films prepared at 100 °C showed the least stress and the largest concentration of charge carriers. Consequently, the concentration of charge carriers produced from the presence of $[Al^{o}_{Zn}]$ is associated with the stress on the film.

Post-deposition annealing can not only reduce the compressive stress, but also form oxygen vacancies. Therefore, the increase of charge carriers in the concentration with annealing is due to the ionization of oxygen vacancies with an ionization factor of 0.1 ± 0.03. The variation in the compressive stress of 1.61 GPa to 0.20 GPa with heat-treatment did not appear to affect the substitution of Zn with Al.

ACKNOWLEDGMENT

The study was supported by in Inha Research Grant 2010.

REFERENCE

1. K. L. Chopra, S. Major, and D. K. Pandya, *Thin Solid Films* **102**, 1 (1983).
2. S. A. Aly, N. Z. El Sayed, and M. A. Kaid, *Vaccum* **61**, 1 (2001).
3. S. Major and K. L. Chopra, *Sol. Energ. Mater.* **17**, 319 (1988).
4. M. Krunks and E. Mellikov, *Thin Solid Films* **270**, 33 (1995).
5. T. Minami, H. Nato, and S. Takata, *Jpn. J. Appl. Phys.* **24**, L781 (1985).
6. Y. Igasaki and H. Saito, *J. Appl. Phys.* **70**, 3613 (1991).
7. G. A. Hirata, J. Mckittrick, J. Siqueros, O. A. Lopez, T. Cheeks, and O. J. Contreras, *Vac. Sci. Technol. A* **14**, 791 (1996).
8. B. S. Kim, E. K. Kim, and Y. S. Kim, *J. Kor. Ceram. Soc.* **43**, 532 (2006).
9. M. Chen, Z. L. Pei, X. Wang, C. Sun, and L. S. Wen, *J. Vac. Sci. Technol. A* **19**, 963 (2001).
10. M. K. Puchert, P. Y. Timbrell, and R. N. Lamb, *J. Vac. Sci. Technol. A* **14**, 2220 (1996).
11. H. W. Kim and N. H. Kim, *Met. Sci. Eng. B* **130**, 297 (2003).
12. P. Neil, Dasgupta, S. Neubert, W. Y. Lee, O. Trejo, J.-R. Lee, and F. B. Prinz, *Chem. Mater.* **22**, 4769 (2010).
13. S. Takada, *J. Appl. Phy.* **73**, 4739 (1993)
14. D. M. Hoffman, D. Pfisterer J. Sann, B. K. Meyer, R. Tenazaera, V. Munoz-Sanjose, T. Frank, and G. pensl, *Appl. Phys. A* **88**, 147 (2007).
15. H. S. Kim, E. S. Jung, W. J. Lee, J. H. Kim, S.O. Ryu, and S. Y. Choi, *Ceram. Int.* **34**, 1097 (2008).
16. P. Wu, Q. Li, X. Zou, W. Cheng, D. Zhang, C. Zhao, L. Chi, and T. Xiao, *J. Phys. CS* **188**, 012054 (2009).
17. C. J. Xian, J. K. Ahn, N. J. Seong, S. G. Yoon, K. H. Jang, and W. H. Park, *J. Phys. D: Appl. Phys.* **41**, 215107 (2008).
18. M. J. Lee, T. I. Lee, J. H. Lim, J. S. Bang, W. Lee, T. Y. Lee, and J. M. Myoung, *Electron. Mater. Lett.* **5**, 127 (2009).